SCIENTIFIC REPORTS

OPEN

General calibration of microbial growth in microplate readers

Keiran Stevenson[1], Alexander F. McVey[1], Ivan B. N. Clark[2], Peter S. Swain[2] & Teuta Pilizota[1]

Received: 04 July 2016
Accepted: 15 November 2016
Published: 13 December 2016

Optical density (OD) measurements of microbial growth are one of the most common techniques used in microbiology, with applications ranging from studies of antibiotic efficacy to investigations of growth under different nutritional or stress environments, to characterization of different mutant strains, including those harbouring synthetic circuits. OD measurements are performed under the assumption that the OD value obtained is proportional to the cell number, i.e. the concentration of the sample. However, the assumption holds true in a limited range of conditions, and calibration techniques that determine that range are currently missing. Here we present a set of calibration procedures and considerations that are necessary to successfully estimate the cell concentration from OD measurements.

Bacteria and yeast are widely studied microorganisms of great economic, medical and societal interest. Much of our understanding of bacterial and yeast life cycles stems from monitoring their proliferation in time and the most routine way of doing so is using optical density (OD) measurements. The applications of such measurements range from routine checks during different cloning techniques[1]; through studying cellular physiology and metabolism[2,3]; to determining the growth rate for antibiotic dosage[4,5]; and monitoring of biomass accumulation during bio-industrial fermentation[6]. Here we introduce a set of calibration techniques that take into account the relevant parameters affecting OD measurements, including at high culture densities, in a range of conditions commonly used by researchers.

OD measurements have become synonymous with measurements of bacterial number (N) or concentration (C), in accordance with the Beer-Lambert law. However, OD measurements are turbidity measurements[7,8], thus the Beer-Lambert law can be applied, with some considerations, only for microbial cultures of low densities. OD measurements in plate readers, increasingly used for high-throughput estimates of microbial growth, operate predominantly at higher culture densities where OD is expected to have a parabolic dependency on N[8]. Additionally, the proportionality constants (either in low or high density regimes) strongly depend on several parameters, for example cell size, which need to be included in robust calibration techniques. Yet, these techniques, essential when using OD measurements for quantitative studies of microbial growth, including growth rates, lag times and cell yields, have thus far not been established.

The Beer-Lambert law (Supplementary Note 1) assumes that light is only absorbed to derive $OD \sim C$, which is true if the light received by the detector of a typical spectrophotometer is the light that did not interact with the sample in any way[7,9]. In general, when microbial cells are well dispersed in the solution (for the cases where N is small, i.e. single scattering regime) and the geometry of the spectrophotometer is suitable, the Beer-Lambert law is a good approximation for turbidity measurements, and N (or C) is ~OD[7,8]. By the suitable geometry of the spectrophotometer, we mean the likelihood of the scattered light reaching the detector in the spectrophotometer even in the single scattering regime (Fig. 1A,B).

Most bacteria and yeast scatter light at small angles (a few degrees)[10], and, thus, the distance from the scatterer to the detector (d) and the radius (R) of the aperture (Fig. 1A) will determine how close a particular spectrophotometer is to the ideal case, even in the single scattering regime. Supplementary Figure 1A shows measurements taken of the same sample in five different spectrophotometers, indicating that different spectrophotometers need to be cross-calibrated even when used in the single scattering regime[9,11]. As N increases the probability of incident light being scattered by particles multiple times also increases (Fig. 1B), the so-called multiple scattering regime. In this regime the Beer-Lambert law is no longer a suitable approximation, and OD is expected to have a parabolic dependency on N[8]. Similarly, as the probability of multiple scattering events increases even further (i.e. for very high N), light is increasingly deflected away from the detector, and can be described with diffusive

[1]Centre for Synthetic and Systems Biology, School of Biological Sciences, University of Edinburgh, Roger Land Building, Alexander Crum Brown Road, Edinburgh, EH9 3FF, United Kingdom. [2]Centre for Synthetic and Systems Biology, School of Biological Sciences, University of Edinburgh, CH Waddington Building, Mayfield Road, Edinburgh EH9 3JD, UK. Correspondence and requests for materials should be addressed to T.P. (email: teuta.pilizota@ed.ac.uk)

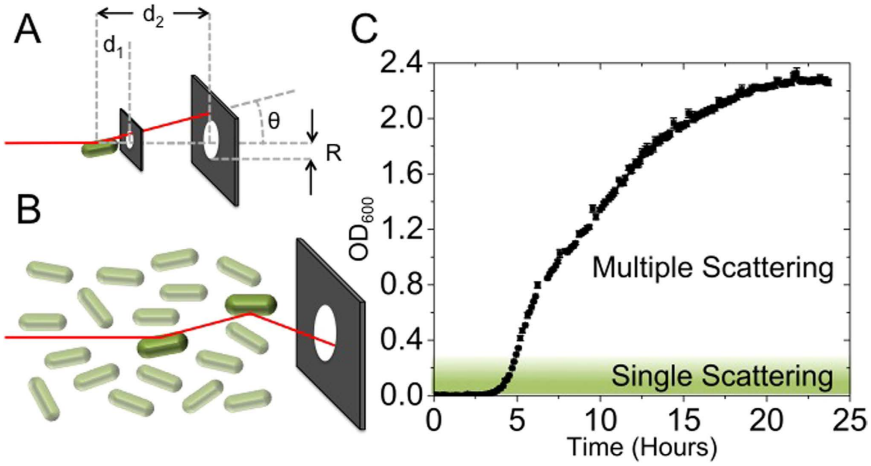

Figure 1. Schematic showing that light incident on a sample is scattered by an angle θ from the optical axis (z), either once as in (**A**) or multiple times (**B**). Single scattering events are more likely to deflect light away from the aperture (radius R), but the effect of this scattering is highly dependent upon the size of the detector and the distance between detector and sample (d_1 or d_2). As the concentration of cells increases, the probability of light being scattered back into the detector is increased. (**C**) A typical OD curve for *E. coli* measured at $\lambda = 600$ nm (for measurements at different λ see Supplementary Fig. 2). The depicted curve is the mean value of ten replicate measurements (performed in separate wells of the same plate in the microplate reader and on independent days and separate plates). Error bars are the standard error of the mean. Where the error bars are not visible, they are smaller then the data symbols. Single and multiple scattering regimes have been indicated with different colour shading. The OD saturates when N is large enough to deplete the nutrient sources in the media.

approximations (the so-called photon diffusion limit)[12,13]. Figure 1C shows a typical OD curve for *Escherichia coli* grown in rich media, with the single and multiple scattering regimes indicated.

In the single scattering regime (small N and $OD_{600} \lesssim 0.2$)[8,13,14], where the Beer-Lambert law ($OD \sim N$) approximately holds, exact solutions to the scattering problem exist[9]. Depending on the size and shape of the scatterer (bacteria or yeast), as well as difference in the index of refraction between the scatterer and the media, various approximations have been used (Supplementary Table 1). For example, the Jöbst approximation, used for spherical bacteria with dimensions comparable to the wavelength of light ($r \sim \lambda$, where r is radius of the bacteria and λ the wavelength of incident light), gives the OD to be proportional to N and r^4 (i.e. bacterial volume to the power of four thirds)[15].

Multiple scattering effects can be incorporated into scattering theory with the inclusion of a correction factor $CF(\sigma, z)$ (Supplementary Note 2), but, unfortunately, to calculate the correction factor, N must be known. Therefore, when using microplate readers in the multiple scattering regime the most practical way of determining the relationship between OD and N is to calibrate. Correct calibration is of particular relevance to high-throughput measurements of quantitative growth rate and cell yield in plate readers and bio-reactors, but it is rarely reported. Additionally, it is often assumed that a single calibration curve for a given instrument is sufficient[16], or calibration is performed by counting colony forming units (CFUs)[17], which only includes live bacteria and is not necessarily suitable for growth under different antibiotics (where cells can be dead, but not lysed). For correct calibration, the shape and size changes of scatterers (bacteria and yeast) as well as index of refraction changes of the media (n_m) and/or of scatterers (n_p) need to be taken into account.

Results

Smaller scatters have higher concentrations for a given OD. To demonstrate the effect of differences in the size of scatterers on OD in the single and multiple scattering regimes, we measured monodisperse solutions of beads with different diameters (D), known index of refraction and known concentrations (C) determined by direct counting in a microscope. Calibration curves for each sample of beads are given in Fig. 2A. For a fixed OD, C increases as the diameter of the scatter decreases (Fig. 2B). The relative effect of C on OD is more pronounced for $D \sim \lambda$, in both the single and multiple scattering regimes, indicating that any changes in size for yeast cultures (with typical cell size ~5 μm) should affect the calibration curve less than those for bacterial cultures (with typical cell size ~1 μm). Similar conclusions also hold true for samples heterogeneous in size. Upon introduction of a polydisperse sample of 0.5 μm and 1.0 μm diameter beads (a 1:1 mixture by volume), C is seen to deviate greatly from both monodisperse solutions (Fig. 2C). Consequently, while the OD versus C calibration curves follow similar trends (a second order polynomial)[8], the exact calibration curve is highly dependent upon D, particularly for $D \sim \lambda$.

Calibration of OD typically changes with growth conditions and cell size. The effects of changing the size of the scatterer seen in bead suspensions are also visible in cultures of *E. coli* and yeast measured in a plate reader (Fig. 3A and Methods). The representative images (Fig. 3B–H) show the change in cell geometry. We obtained different cell sizes for *E. coli* by sampling either at different stages of growth in rich undefined media (Supplementary Fig. S4) or by growing the culture in the presence of a sublethal concentration of ampicillin, a

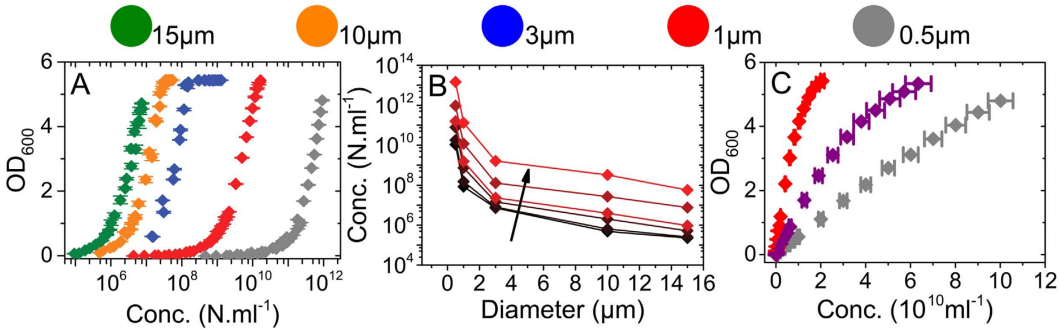

Figure 2. OD measurements of spherical polystyrene bead suspensions. Each set of data (for a given bead size) consists of dilutions of two independently prepared stock solutions whose actual concentration was determined by counting in a microfluidic slide (Methods). For each independently prepared dilution series at least five experimental replicates were performed and plotted as averages with standard errors. Where independent dilution series were prepared for the same bead size these are plotted with the same colour. The differences between independently prepared and counted dilution series for the same bead size are so small that the data overlap. Any error bars that are not visible are smaller then the data symbols. Bead size corresponds to the diagram above the graphs ($0.51 \pm 0.01\,\mu m$, $0.96 \pm 0.07\,\mu m$, $3.00 \pm 0.07\,\mu m$, $10.0 \pm 0.6\,\mu m$ and $15.7 \pm 1.4\,\mu m$) and bead index of refraction is $n_p = 1.59$. Representative images of beads used for *C* measurements are shown in Supplementary Figure 3. (**A**) Comparison of concentrations (Methods) and measured OD in a microplate reader for a given bead diameter. (**B**) The bead concentration as a function of *D* obtained from (**A**) for the following ODs: 0.05, 0.1, 0.5, 1 and 10. Increasing OD is represented as increasing brightness of red and by the arrow. (**C**) Measurements of 0.5 μm; 1.0 μm bead suspensions and the resultant (1:1 by volume) mixture in purple.

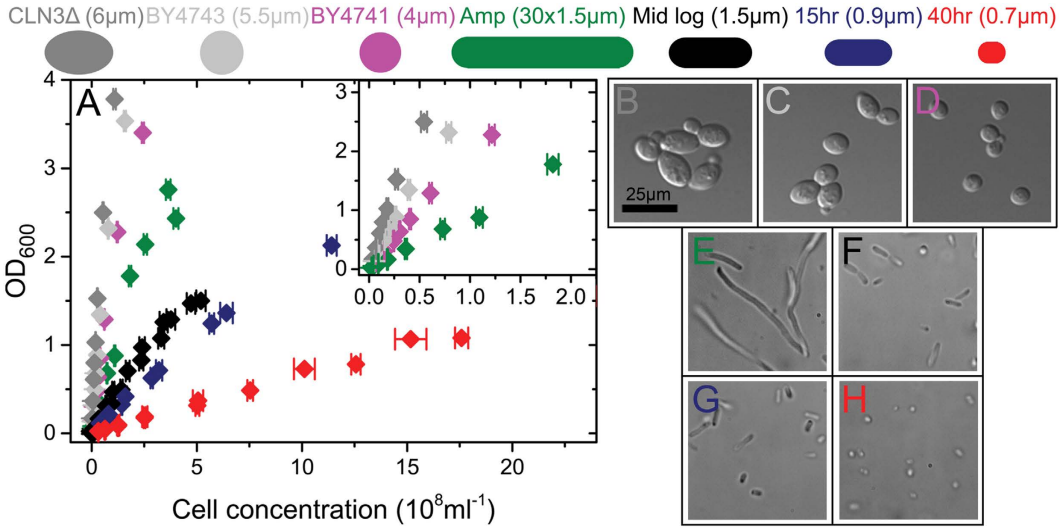

Figure 3. (**A**) OD vs. *C* is shown for yeast diploids (grey); yeast haploid (purple); filamentous (green) and mid-log (black) *E. coli*; and early (blue) and late (red) stationary phase *E. coli* using dilutions of at least two cell stock solutions prepared from cells grown on different days. Actual cell concentrations were determined by counting in a microscope. For each independently prepared dilution series at least five experimental replicates were performed and are plotted as averages with standard errors. Independent dilution series that were prepared for the same cell size are plotted with the same colour. For cells of the same size, the differences between independently prepared and counted dilution series are so small that the data overlap. Error bars that are not visible are smaller then the data symbols. (**B**–**H**) Representative images of each culture obtained during microscopy. The scale bar is shown in B and applies to all panels. (**B**) Yeast CLN3Δ homozygous diploid mutant (**C**) Yeast diploid, (**D**) Yeast haploid. (**E**) *E. coli* cells grown in the presence of sub lethal concentration of ampicillin to induce filamentation. (**F**) *E. coli* cells grown to mid log phase in LB (OD = 0.2). (**G**) *E. coli* cells at early stationary phase (OD = 2.3), (**H**) *E. coli* cells at late stationary phase (after 40 hr).

β-lactam antibiotic that inhibits the formation of the cell wall. Ampicillin induces filamentation[18,19] (Fig. 3E), a property shared by many other stresses (including the antibiotic groups cephalosporins and quinolones[20] and UV

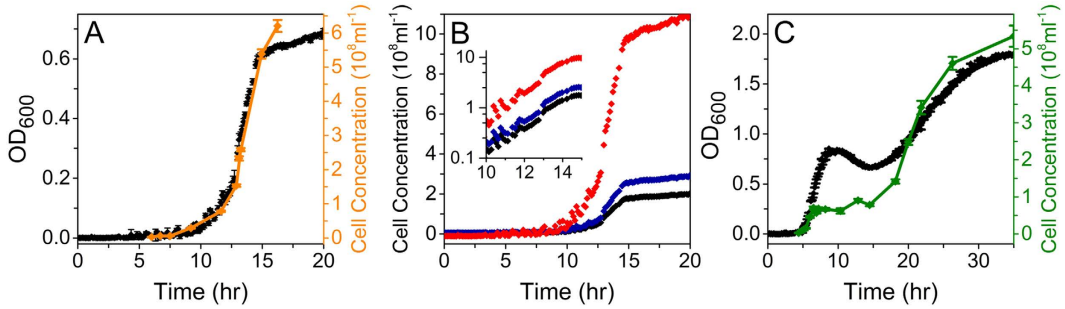

Figure 4. Growth curves and cell counts. (**A**) OD (black) and cell concentration (orange) during growth of *E. coli* in MM9 with glucose. OD and *C* are correlated until starvation when cell size is no longer constant. (**B**) The OD curve from (**A**) converted to cell concentration using the the mid-log (black), 15 hr (blue) and 40 hr (red) curves in Fig. 3A. Calibration performed on cells of different sizes produces substantial differences in cell concentration. (**C**) OD (black) and cell concentration (green) in LB with 9 Ampicillin. The lack of correlation between OD and *C* is caused by antibiotic induced filamentation and filaments of fluctuating length during growth. For (**B**) and (**C**), the OD curve shown is an average with standard errors of 10 independent experimental replicates. Each cell concentration point is an average count with the standard error obtained from counting 20–50 independent fields of view in a microscope (*Methods*).

irradiation and oxidative damage[21]). We obtained different sizes of yeast cells by using three different strains (wild type haploid and diploid and a diploid mutant exhibiting increased cell size)[22].

Each chosen scatterer in Fig. 3 exhibits a different relationship between OD and *C*. In particular, the calibration curve obtained using filamentous cells is considerably altered compared to the rest of the *E. coli* samples. The differences in the calibration of the yeast samples (as *D* increases from 4 μm to 6 μm) are smaller compared to those of the bacterial cultures.

The effects of changes in the calibration curve during a single growth curve are demonstrated in Fig. 4 and Supplementary Figure 5 by counting the cell concentration in parallel with measuring the OD. We first show that if the cell size does not change during the growth of the culture, the calibration curve maintains a parabolic dependency on *N* (Fig. 4A). To maintain a constant cell size, we grew *E. coli* in MM9 with glucose as the sole carbon source (Methods). Under these conditions OD and *C* are correlated throughout the exponential growth, only diverging at 15 hr when the carbon source is depleted and the cells enter stationary phase and reduce in volume. Nevertheless, if cells change size during growth, for example when growing on rich undefined media (Supplementary Fig. 5), the calibration curve will change in time as well. To demonstrate the effect of using calibration curves obtained for cells of different sizes, in Fig. 4B we show the OD curve from Fig. 4A converted to *C* using three different calibrations curves. *C* is substantially altered depending on the calibration curve selected, with the effect on the lag time and final cell yield being particularly pronounced.

To further demonstrate the effect on changes in cell size throughout the growth curve we grew *E. coli* under sublethal concentrations of ampicillin (Fig. 4C). A substantial deviation between OD and *C* is visible. During the initial part of the log phase OD and *C* show the same time dependency. At OD ~ 0.2, however, *N* remains roughly constant while the OD increases. This increase in OD for constant *N* is the result of an increase in cell mass (as cells filament and increase in size), rather than increasing *N* (Fig. 3E). The decrease in OD at constant *N* (10 hr) is most likely the result of division of filaments into smaller cells. 15 hr after culture inoculation, both *N* and OD increase again as filamentous bacteria both divide and grow as smaller cells.

There can be a substantial difference between the expected OD and *C* relationship for scatterers of a fixed size and those whose size changes during growth. For example, in Supplementary Figure 5 we show comparison of OD and *C* from Fig. 4A and 4C. For a constant cell size (Supplementary Fig. 5A), the calibration curve follows the same second degree polynomial expected from Figs 2A and 2C and 3A, whereas for growth in LB+ampicillin, where cell size changes, the calibration curve is more complex (Supplementary Fig. 5B). Supplementary Figure 6 shows the difference between growth rates obtained from non-calibrated OD and *C* measurements for the same cell culture. The value and time point at which maximum growth rate is reached in Supplementary Figure 6A (corresponding to Fig. 4A) are similar, whereas Supplementary Figure 6B shows that maximum growth rate obtained from Fig. 4C is reached several hours before the maximum growth rate obtained from OD measurements. Additionally, Supplementary Figure 6B shows that the two values differ significantly, by a factor of two.

Calibration changes with the refractive index of the growth media. Apart from the size of the scatterer, changes in the difference between refractive index of the growth media (n_m) and the refractive index of the scatterer (n_p) can have a significant effect on the OD calibration curve. For example, we changed n_m by the addition of sucrose, while keeping the refractive index of the scatterer (1 μm bead) the same (Supplementary Fig. 7). As the relationship $n = \frac{n_p}{n_m}$ decreases, the OD of a fixed *N* is similarly reduced. The effect is small for beads as the relative difference between n_p and n_m is large, but will be more pronounced for biological samples like bacteria, which have a smaller *n* (Supplementary Table 2).

Finally, we investigated the effect of bacterial lysis and intracellular matter leaking into the media on n_m, which can occur during growth under antibiotics. We measured the refractive index of LB media with different

concentrations of lysed *E. coli* cells. The intracellular material (Supplementary Table 3 and Supplementary Fig. 8), released into the media from high concentrations of cells (as high as $2 \cdot 10^9 ml^{-1}$ cells) results in only a small increase in n_m. The increase is substantially lower than n_m variations caused by the introduction of even low concentrations of sucrose to ddH_2O (Supplementary Fig. 8). Thus, cell lysis as a result of growth under different antibiotics will unlikely change n_m sufficiently to alter the OD versus *C* calibration curve. Nevertheless, growth at high sugar concentrations, such as in the food industry, will.

Discussion

We have presented potential issues and the calibration protocols needed for quantitative measurements of microbial growth rates based on OD measurements. We show that different spectrophotometers and microplate readers need to be cross-calibrated to compare the OD readings as an absolute number. Furthermore, variations in diameter *D* and refractive index of the cell or of the media need to be considered and calibrated to avoid substantially over- or underestimating the number of cells present in the sample. Therefore, we recommend first determining if considerable changes in cell size are expected during growth of the culture. If not, and size is expected to remain constant, calibration of OD against *N* needs to be performed once for each *D* and index of refraction, and ideally reported in publications. The closer the *D* of the scatterer to λ, the more important it is to perform calibration of OD against *N* for each different cell size. Changes in refractive index can be particularly relevant during growth in media with high sugar concentrations (such as those in food sciences[23–26] and drinks with high osmolarity like beer). We have shown that changes in n_m due to lysis induced leakage of cell material, for example when grown in the presence of antibiotics, are small. However, we note that the effect of changing media index of refraction is likely to be more pronounced in bioreactor experiments where *C* is far larger. If cell size is expected to change substantially during the course of growth of the microbial culture (for example: growth under antibiotics or various other stresses, growth of shape-inducing mutants, growth of over-expression strains, and growth of strains that induce chains or clumps), OD measurements are no longer suitable and direct counting of *N* should be performed, using, for example, microscopy.

Methods

Bacteria cultures. All bacterial cell culture studies were conducted using *E. coli* BW25113 (F^-, DE(araD-araB)567, lacZ4787(del)::rrnB-3, LAM^-, rph-1, DE(rhaD-rhaB)568, hsdR514), a close relative of MG1655, with plasmid pWR20 which expresses and enhanced GFP for cytoplasmic volume monitoring[27]. All experiments were conducted in LB media except where explicitly stated. MM9 medium contained 0.1% Glucose, no amino acids and 20 mmol KCl. MM9 (Modified M9) is of the same composition as M9[28] except sodium phosphate buffer only was used. Where cells were grown with antibiotics, $9 \mu g\ ml^{-1}$ Ampicillin was added to the culture medium before the addition of cells.

Yeast cultures. Yeast studies used three S288c-derived strains: BY4741, BY4743[29] and the cln3 homozygous deletion derived from the *Saccharomyces* genome deletion project[30]. Cells were cultured at 30 °C in YPD media, containing 2% glucose.

Colloidal bead cultures. Colloidal bead cultures were created using dilutions of polystyrene beads of known diameter (*D*) $0.51 \pm 0.01 \mu m$ (Polysciences), $0.96 \pm 0.07 \mu m$ (Bangs Laboratory), $3.00 \pm 0.07 \mu m$, $10.0 \pm 0.6 \mu m$ and 15.7 ± 1.4 (all Polysciences) and known index of refraction ($n_p = 1.59$) in ddH_20. At each *D*, a dilution series was performed, to produce samples of known concentrations (*C*) between 10^5 and 10^{12} *N* ml^{-1}. For all samples *C* was experimentally determined by counting the number of beads in 10 of the dilution in a microscope tunnel slide[27].

Optical density measurements. OD measurements of bacterial and colloidal bead cultures were performed in a Spectrostar Omega microplate reader (BMG, Germany) with a Costar Flat Bottom 96-well plate with lid and $200 \mu l$ per well ($300 \mu l$ for data in Fig. 4). Absorbance was measured at wavelength 600 and temperature 37 °C and the mean of 5 readings taken. For bacterial cultures, 30 wells were grown to OD = 0.15 in MM9 medium. The wells were pooled and $125 \mu g\ ml^{-1}$ chloramphenicol was added to inhibit further cell division or growth. The cells were then diluted in increments to provide a range of OD readings. A single dilution of cells for each series was then imaged in the brightfield microscope as above for the polystyrene beads. All measurements in the main text were reported using the BMG with correction values, which is given as the measured OD multiplied by 1.0560 for $300 \mu l$, 1.5848 for $200 \mu l$ and 6.3694 for $100 \mu l$.

OD measurements for yeast cultures were performed in a Tecan M200 fluorescent spectrophotometer, using a Costar Flat Bottom 96-well plate with lid and $200 \mu l$ per well for all measurements. Cells were cultured for 16 hr in YPD media and dilutions for measurement made in the same media. Duplicate OD measurements were taken at 600 nm (bandwidth 9) with 15 flashes at 30 °C. Yeast cell counts were performed using a Neubauer improved bright-line haemocytometer (Marienfeld).

Calibration between the two spectrophotometers was performed using *E. coli* grown in LB to mid log as in Fig. 3A black and the OD measured in both platereaders. The relative difference in measurements was then calculated and used to correct the data gathered for yeast. The calibration is shown in Supplementary Figure 1B.

Brightfield Microscopy. Imaging of samples was performed using a custom-built brightfield microscope consisting of a 100× oil immersion objective lens (Nikon) with the sample mounted on a Nano-LP200 piezoelectric stage (Mad City Labs). Illumination of the sample was provided by a white LED (Luxeon Star) and images recorded on an iXon Ultra 897 EMCCD camera (Andor). Stacks of images through each sample were acquired every 0.05 s and separations of $1 \mu m$, ensuring all scatterers in the volume were identified without introducing overcounting. True values of *C* were experimentally determined by counting *N* present in the known stack

volume determined by the field of view of the microscope ($55.6 \times 55.6 \times 100\,\mu m$). For each each bead preparation in Fig. 2 between 20–50 independent fields of view were counted. Similarly, for each cell preparation in Fig. 3 we counted 20–50 independent fields of view. For each bead or cell size given in Figs 2 and 3, we used at least two independent stock solutions/cultures (from which dilution series were prepared). In Fig. 4A and C each concentration of cells was counted independently, again using 20–50 independent fields of view.

Osmolarity measurements. For osmolarity measurements, beads ($D = 1\,\mu m$) were diluted from manufacturer stock solution into ddH_2O and then further diluted into solutions of 0 mOsm, 116 mOsm, 231 mOsm, 463 mOsm and 925 mOsm (achieved by diluting sucrose (Sigma) in ddH_2O) to produce concentrations in media of refractive index $n_m = 1.333$; 1.339; 1.344; 1.353 and 1.368 respectively. For each osmolarity, C was determined by counting N using brightfield microscopy as above. Osmolalities were measured using a freezing point depression osmometer (Camlab).

Fitting of bead optical density measurements. Fitting of the data presented in Fig. 2A was performed in the Matlab[31] environment utilising the built in curve fitting tools. Data was first trimmed to remove points where the spectrophotometer had saturated then fitted as a 2nd degree polynomial with robust fitting using the bisquare method. The polynomials found are presented in Supplementary Table 4. These polynomials were then solved for OD = 0.05, 0.1, 0.5, 1 and 10 to give the traces presented in Fig. 2C.

***E. coli* cell concentration monitoring during growth curves.** In order to determine C during batch culture growth, cells were added to 10 ml of the experimental media, which was then divided among 30–60 wells of a 96-well plate. The cells were grown at 37 °C and OD measured every 7.5 min. When an increase in OD above the baseline was observed sampling for C began, with each new sample taken from a separate well. For all growth curves at least 8 wells were left untouched to provide a complete growth curve for comparison. In the rare cases where the growth curve deviated significantly from the average, those traces were excluded from all measurements. $125\,\mu g\ ml^{-1}$ chloramphenicol was added to samples taken from the plate to arrest all cell division and growth. Samples were then imaged under brightfield illumination and N counted manually to determine C for each time point. At OD > 0.2 samples were diluted in the culture medium to reduce cell overlap in the slide. For Fig. 4 the two data sets were aligned by using a least squares method to determine the scales of both axes, minimising the sum of: $(\frac{Y_{chase}}{c} - Y_{OD})^2$ where c is the scaling factor. For Supplementary Figure 5 solid and dashed fits were produced using 1st and 2nd degree polynomials respectively. The fitted region for each was selected by expanding sequentially from zero until the fit quality started to drop.

Refractive index measurements. *E. coli* cells (strain MG1655) were grown in LB to OD = 0.3, spun down and concentrated 33.3× before being subjected to sonication to lyse the cells. This cell lysate was diluted to 0.0625×, 0.125×, 0.25×, 0.5× and 1× concentrations and the refractive index measured. The original cell extract was counted as above to determine the concentration of cells before lysing. DNA was obtained as 23-mer primers (Sigma-Aldrich) suspended in ddH_2O, with concentration measured using a NanoDrop (ThermoScientific). Refractive indices of solutions were measured in a manual refractometer (Bellingham and Stanley, London). Sucrose data was obtained from a standard brix index[32].

Raw data. Raw data generated as part of this work is available at http://datashare.is.ed.ac.uk/handle/10283/2063 (Figs 1, 2 and 3) and http://datashare.is.ed.ac.uk/handle/10283/2064 (Fig. 4).

References

1. Neidhardt, F. C. *Escherichia coli and Salmonella: Cellular and Molecular Biology* (ASM, 1996).
2. Klumpp, S., Zhang, Z. & Hwa, T. Growth Rate-Dependent Global Effects on Gene Expression in Bacteria. *Cell* **139,** 1366–1375 (2009).
3. Scott, M., Gunderson, C. W., Mateescu, E. M., Zhang, Z. & Hwa, T. Interdependence of Cell Growth and Gene Expression: Origins and Consequences. *Science* **330,** 1099–1102 (2010).
4. Andrews, J. M. Determination of minimum inhibitory concentrations. *J Antimicrob Chemoth* **48,** 5–16 (2001).
5. Bollenbach, T., Quan, S., Chait, R. & Kishony, R. Nonoptimal Microbial Response to Antibiotics Underlies Suppressive Drug Interactions. *Cell* **139,** 707–718 (2009).
6. Mahalik, S., Sharma, A. K. & Mukherjee, K. J. Genome engineering for improved recombinant protein expression in *Escherichia coli*. *Microb Cell Fact* **13,** 177 (2014).
7. Koch, A. L. Some Calculations on the Turbidity of Mitochondria and Bacteria. *Biochim Biophys Acta* **51,** 429–441 (1961).
8. Koch, A. L. Turbidity measurements of bacterial cultures in some available commercial instruments. *Anal Biochem* **38,** 252–259 (1970).
9. Koch, A. L. Theory of the angular dependence of light scattered by bacteria and similar-sized biological objects. *J Theor Bio* **18,** 133–156 (1968).
10. Koch, A. L. & Ehrenfeld, E. The size and shape of bacteria by light scattering measurements. *Biochim Biophys Acta* **165(2),** 262–273 (1968).
11. Koch, A. L. Distribution of Cell Size in Growing Cultures of Bacteria and the Applicability of the Collins-Richmond Principle. *J. Gen. Microbiol.* **45(3),** 409–417 (1966).
12. Zaccanti, G., Del Bianco, S. & Martelli, F. Measurements of optical properties of high-density media. *Appl Opt* **42(19),** 4023–4030 (2003).
13. Ishimaru, A. Approximate solutions for tenuous media in *Wave Propagation and Scattering in Random Media*. (Wiley-IEEE Press, 1997).
14. Giusto, A. *et al.* Optical properties of high-density dispersions of particles: application to intralipid solutions. *Appl Opt* **42(21),** 4375–4380 (2003).
15. Baranyi, J. Comparison of Stochastic and Deterministic Concepts of Bacterial Lag. *J Theor Biol.* **192,** 403–408 (1998).

16. Warringer, J. & Blomberg, A. Automated screening in environmental arrays allows analysis of quantitative phenotypic profiles in Saccharomyces cerevisiae. *Yeast* **20(1),** 53–67 (2003).
17. Jung, J. H. & Lee, J. E. Real-time bacterial microcolony counting using on-chip microscopy. *Sci Rep* **6,** 21473 (2016).
18. Buijs, J., Dofferhoffa, A. S. M., Moutona, J. W., Wagenvoorta, J. H. T. & van der Meer, J. W. M. Concentration-dependency of β-lactam-induced filament formation in Gram-negative bacteria. *Clin Microbiol Infec* **14(4),** 344–349 (2008).
19. Miller, C. SOS response induction by beta-lactams and bacterial defense against antibiotic lethality. *Science* **305(5690),** 1629–1631 (2004).
20. Diver, J. M. & Wise, R. Morphological and biochemical changes in Escherichia coli after exposure to ciprofloxacin. *J. Antimicrob. Chemother.* **18,** 31–41, Supplement D (1986).
21. Yao, Z., Kahne, D. & Kishony, R. Distinct single-cell morphological dynamics under beta-lactam antibiotics. *Mol. Cell* **48(5),** 705–12 (2012).
22. Jorgensen, P., Nishikawa, J. L., Breitkreutz, B. J. & Tyers, M. Systematic identification of pathways that couple cell growth and division in yeast. *Science* **297,** 395–400 (2002).
23. Offersgaard, J. F. & Öjelund, H. Correction of Nonlinear Effects in Absorbance Measurements. *Appl Spectrosc* **56,** 469–476 (2002).
24. Prüß, B. M., Nelms, J. M., Park, C. & Wolfe, A. J. Mutations in NADH:Ubiquinone Oxidoreductase. *J Bacteriol* **176(8),** 2143–2150 (1994).
25. Sezonov, G., Joseleau-Petit, D. & D'Ari, R. Escherichia coli physiology in Luria-Bertani broth. *ASM* **189**(**23**), 8746–8749 (2007).
26. Zhao, L., Zhang, H., Hao, T. & Li, S. *In vitro* antibacterial activities and mechanism of sugar fatty acid esters against five food-related bacteria. *Food Chemistry* **187,** 370–377 (2015).
27. Pilizota, T. & Shaevitz, J. W. Plasmolysis and cell shape depend on solute outer-membrane permeability during hyperosmotic shock in *E. coli*. *Biophys J* **104(12),** 2733–2742 (2013).
28. Cold Spring Harbour Laboratory. M9 minimal medium (standard). *Cold Spring Harb Protoc*, doi: 10.1101/pdb.rec12295 (2010).
29. Brachmann, C. B. *et al.* Designer deletion strains derived from Saccharomyces cerevisiae S288C: a useful set of strains and plasmids for PCR-mediated gene disruption and other applications. *Yeast* **14(2),** 115–32 (1998).
30. Winzeler, E. A. *et al.* Functional characterization of the S. cerevisiae genome by gene deletion and parallel analysis. *Science.* **285(5429),** 901–906 (1999).
31. The MathWorks Inc. *MATLAB and Statistics Toolbox Release 2015b* (The MathWorks Inc, Natick, Massachusetts, United States). (2015).
32. Snyder, C. F. & Hattenburg, A. T. *Refractive indices and densities of aqueous solutions of invert sugar.* Washington D.C. USDoC, National Bureau of Standards. http://digital.library.unt.edu/ark:/67531/metadc70449/ Accessed: 20 June 2016.

Acknowledgements

KS is supported by the BBSRC iCASE grant to TP. AFM, IBNC, PSS and TP acknowledge the support of UK Research Councils Synthetic Biology for Growth programme and KS, AFM, IBNC, PSS and TP are members of a BBSRC/EPSRC/MRC funded Synthetic Biology Research Centre. TP acknowledges the support of BBSRC CBMNet grant. We thank Jerko Rosko, Dejan Kunovac and all other members of the Pilizota and Swain lab for their comments and support, Andrew Schofield for granting us access to the refractometer and Meriem El Karoui and Rosalind Allen for helpful comments and discussions.

Author Contributions

T.P. and K.S. designed the study. T.P., K.S. and P.S.S. conceived the experiments. T.P., K.S. and I.B.N.C. performed the experiments and analysed the data. K.S., A.F.M. and T.P. interpreted the data and wrote the paper. All authors reviewed the manuscript.

Additional Information

Supplementary information accompanies this paper at http://www.nature.com/srep

Competing financial interests: The authors declare no competing financial interests.

How to cite this article: Stevenson, K. *et al.* General calibration of microbial growth in microplate readers. *Sci. Rep.* **6**, 38828; doi: 10.1038/srep38828 (2016).

Publisher's note: Springer Nature remains neutral with regard to jurisdictional claims in published maps and institutional affiliations.